Clim. Past Discuss., 7, 153–198, 2011
www.clim-past-discuss.net/7/153/2011/
doi:10.5194/cpd-7-153-2011

Climate of the Past Discussions

A millennial multi-proxy reconstruction of summer PDSI for Southern South America

É. Boucher[1], **J. Guiot**[1], **and E. Chapron**[2]

[1]Centre Européen de Recherche et d'Enseignement des Géosciences de l'Environnement (CEREGE), UMR 6635, Europôle Méditerranéen de l'Arbois, 13545 Aix-en-Provence cedex 4, France
[2]ISTO UMR 6113 Université d'Orléans, 1A rue de la Férollerie, 45071 Orléans cedex 2, France

Received: 21 December 2010 – Accepted: 5 January 2011 – Published: 17 January 2011

Correspondence to: É. Boucher (boucher@cerege.fr)

Published by Copernicus Publications on behalf of the European Geosciences Union.

Abstract

We present the first highly resolved millennial reconstruction of the summer (DJF) Palmer Drought Severity Index (PDSI) for the Southern Hemisphere. Our multi-proxy reconstruction focuses on Southern South-America (SSA, south of 20° S) and is based on a novel spectral analogue method that aims at reconstructing the low frequencies of PDSI series independently from higher frequencies. The analysis of past regimes and long-term fluctuations in the PDSI reveals considerable geographical and temporal variations over the last millennia in SSA. Hence, recent changes, although some were very significant, were rarely exceptional over the last thousand years. However, from the point of view of extremes, recent PDSI values associated to extreme droughts (e.g. in the Andes) or wet spells (e.g. in the Pampas) were unequalled over the last thousand years. A major feature of our reconstruction is that it highlights that low frequency water availability fluctuations in Patagonia were generally in antiphase with those found on the rest of the sub-continent. We show that such antiphases within SSA's hydroclimate could be attributed the Antarctic Oscillation (AAO). The AAO was an important climatic driver during the calibration period (1930–1993) in SSA, and possibly over the last millennia as well. ENSO and PDO signals are also embedded, to a lesser extent, within the PDSI series, but the influence of these forcings has considerably varied through time and space over the last thousand years. Our results therefore highlight the complexity of water-availability fluctuations in SSA and their important dependence on external ocean-atmospheric forcings.

1 Introduction

Numerous evidences exist to support an increasing trend in the severity and intensity of both extremely dry and wet spells, over the last century, in Southern South-America (SSA) (Trenberth et al., 2007; Magrin et al., 2007). These episodes have among the costliest impacts on the economy, society and natural environment in the

CPD
7, 153–198, 2011

area. However, the analysis of present-day climate has shown that an important geographical variability also exists regarding these trends. Indeed, some parts of SSA like Northern Patagonia are actually experiencing a wetter climate by comparison to the conditions that prevailed at the beginning of the 20th century (Garreaud et al., 2009; Dai et al., 2004; Magrin et al., 2007). By contrast, Southern Chile, South-West Argentina and Southern Peru recorded a clear decline in the amount of precipitation (sometimes accompanied by an increase in summer temperatures) during the same period (Magrin et al., 2007). This variability originates mostly from (1) the presence of the Andes cordillera that creates strong W-E climatic contrasts, (2) the important latitudinal, longitudinal and altitudinal gradients over the continent and (3) the notable influence of high latitude and tropical processes such as the Antarctic Oscillation (AAO), El Niño-Southern-Oscillation (ENSO) and the Pacific Decadal Oscillation (PDO) on precipitation distribution and abundance (Garreaud, 2007). Given this variability and the numerous factors of modulation involved, it becomes crucial to place the recent climatic trends in a broader spatio-temporal perspective in order to determine whether or not they have an exceptional character.

Whereas instrumental records are usually too short and scarce to perform such an analysis, highly resolved multi-proxy reconstructions can be useful to place recent climatic trends in a larger temporal or spatial perspective. Most notably, they allow to compare the recent trends with well-known climatic periods such as the Medieval Warm Period (MWP) or the Little Ice Age (LIA) and to place the local patterns of change into a continental, hemispheric or even global perspective. More importantly, such reconstructions can help precise and explain the patterns and mechanisms of climate change in the past. Yet, most efforts have focused on reconstructing past temperatures in the Northern Hemisphere (Bradley and Jones, 1993; Jones et al., 1998; Mann et al., 1998, 1999; Briffa et al., 2002; Moberg et al., 2005) owing to the number of available proxies and the density of high quality instrumental data. In SSA, the first highly resolved multi-proxy temperature and precipitation reconstructions were performed recently (Neukom et al., 2010a,b). The summer temperature reconstruction showed that

CPD
7, 153–198, 2011

the MWP (9th to 14th century) was generally warmer than the last century's average. Complementarily, the precipitation reconstruction covered the last 500 years and showed that summer and winter precipitation behaved in opposite directions over the last centuries (summer precipitations increased since the Little Ice Age, while winter temperatures decreased). However, despite these findings, it remains clear that the continental hydrological balance itself (i.e. the linkages between water inputs, storage, and outputs) is affected by all these parameters synergically. Thus, the reconstruction of an individual parameter (either temperature or precipitation) does not yield a full representation of past water availability fluctuations. Moreover, moisture conditions depend not only on precipitation and temperatures occurring during the season of interest, but also on antecedent moisture conditions. Thus, to better describe water availability fluctuations, one has to take into account both water supply and demand at the earth's surface and evaluate the changes considering prior conditions.

The Palmer Drought Severity Index (Palmer, 1965) is a prominent index that incorporates antecedent moisture conditions and has been extensively used to monitor past droughts and wet spells in the US and elsewhere (Apipattanavis et al., 2009). It has also commonly been reconstructed from dendrochronology mostly in North-America (Cook et al., 1999, 2004; Woodhouse and Overpeck, 1998; Woodhouse and Brown, 2001) and in the Mediterranean basin (Nicault et al., 2008). In SSA, Christie et al. (2009) have used tree rings to reconstruct high frequency variations of the PDSI in the Temperate Mediterranean Transition in the Andes over the last 600 years. However, as for temperature and precipitation, the PDSI needs to be reconstructed at larger spatial (i.e sub-continental) and temporal (i.e millennial) scales in order to place the recent changes in water availability into a broader perspective. Our work therefore focused on reconstructing austral summer (DJF) PDSI values from a multi-proxy approach. We also aimed at reconstructing the full spectra of PDSI variations and at analyzing the possible role of ocean-atmosphere forcings (AAO, ENSO, PDO) on large-scale and long-term PDSI variations in SSA.

CPD
7, 153–198, 2011

2 Data and modeling approach

2.1 PDSI

This work aims at producing millennial gridded reconstructions of the Palmer Drought Severity Index (PDSI, Palmer, 1965) in SSA (south of 20° S). The PDSI is a climatic metric that measures the departure towards abnormally dry or wet conditions (relatively to average conditions). Three input variables are required to calculate the PDSI: monthly precipitation, monthly temperatures and the available water content of soils. Within the calculation of the PDSI, moisture supply and demand are approximated in a simple hydrological accounting model that evaluates evapotranspiration, soil recharge, runoff, and moisture losses from the surface layer (see Palmer, 1965 for original equations). The PDSI produces monthly indexes of meteorological droughts that account for both contemporary and antecedent climatic conditions. The PDSI fluctuates between −10 (extremely dry) and 10 (extremely wet), with 0 corresponding to the local average conditions. The PDSI should be regarded as an approximation of dryness or wetness conditions rather than as an absolute value, as many factors like solar irradiation or aerosol concentrations are not considered explicitly.

In the present paper, we use the gridded (2.5°×2.5°) PDSI dataset computed by Dai et al. (2004) (Fig. 1a) and propose to extend it to the last millennia in SSA. This dataset covers the 1870–2004 period and was calculated from long temperature (CRUTEM2, Jones and Moberg, 2003) and precipitation (Dai et al., 1997; Chen et al., 2002) series.

We provide reconstructions of the summer PDSI for four climatically contrasted regions (Fig. 1a): Patagonia (PG), the Pampas (PM), Sub-Tropical SSA (ST) and the Andes (ANDES). In each region, the climate is driven by similar mechanisms and the evolution of summer PDSI has been relatively uniform over the last decades (see the results section). PG's climate is largely influenced by the low-level westerly flow of the Southern Hemisphere (Garreaud et al., 2009). Westerlies are strongest during the austral summer and constitute an important migratory corridor for the passage of cyclones and anticyclones in the area. By contrast, PM has a relatively dry climate owing

CPD
7, 153–198, 2011

to the subsidence of large air masses on the eastern side of the Andes. However, PM's climate becomes wetter on the Atlantic coast. ST's climate is mainly governed by the position of the Intertropical Convergence Zone (ITCZ) and is characterized by a monsoon-like climate. During the austral summer, large zones of convective precipitations extend to the southernmost portion of the Amazon Basin and over Northern Argentina. The ANDES is the most contrasted zone. The strip of land between the coast and the mountains is very arid, owing to the subsidence of air masses in the area, but the western slope of the Andes receives important orographic precipitation, as low-level winds reach higher altitudes.

2.2 Proxies

To achieve the PDSI reconstructions, we adopted a frequency-dependent approach similar to the one used by Moberg et al. (2005) where each proxy is used only to reconstruct the periodicities for which it provides reliable information (see Sect. 2.4 for details). Thus, a large proxy dataset was compiled from high- and low-resolution proxies (Table 1, Fig. 1b,c). High-resolution proxies are mostly tree rings, (most of which are available on the International Tree Ring Data Bank – ITRDB). We kept only the tree ring series that were longer than 250 years, giving a total of 82 average series. In order to circumvent the well known problems associated to the standardization of tree ring series and the problematic interpretation of medium to low frequency variations (Esper et al., 2002, 2004), we retained only the high frequency variations contained within these series. Low frequencies were removed in each tree-ring chronologies using a low-pass filter (based on the Fast Fourier Transform procedure). Basically, we removed all periodicities below a 12 year threshold (f=0.08). In order to avoid the over-representation of tree ring series in the multi-proxy reconstruction, we selected the first 7 PC's explaining about 30% of the variance of the high frequency tree ring series. Marine sediments from the Cariaco Basin (Black et al., 2007) and lake sediments from the laguna Aculeo (von Gunten et al., 2009) complemented the set of high-resolution proxies. Low-resolution proxies included Andean (Vimeux et al., 2009) and Antarctic

CPD
7, 153–198, 2011

(Goosse et al., 2004) ice cores, Lago Frias sediments (Chapron, unpublished) and Potrok lake sediments (Haberzettl et al., 2005). The Frias sequence is a new sedimentary record from a varved proglacial lake (Ariztegui et al., 2007) draining the Frias River Valley. The Frias sequence consist in a detailed record of goethite content measured every 0.5 cm by sediment diffuse reflectance on a 187 cm long core retrieved in 2008 within Lago Frias main basin. The chronology (Fig. A1) has been established back to AD 1657 by varve counting on digital core images and by the identification of three mass wasting deposits induced by historical large earthquakes in AD 1960; AD 1751 and AD 1737. Geothite content in these annually laminated fine-grained sediments reflect soil erosion after rainfall. Sediments from Cariaco Basin and Laguna Aculeo were used for their low-frequency component as well.

2.3 Analogue method (AM)

The analogue method (Guiot et al., 2005) is commonly used to infill proxy-climate matrix containing missing values. The AM procedure aims at identifying, for each year i in the past where no PDSI value exists, the year k within the instrumental record that has the most "similar" proxy vector. Here, similarity (d^2_{ik}) is measured as an Euclidian distance (Guiot et al., 2005):

$$d^2_{ik} = m^{-2}_{ik} \sum_{j=1}^{m} \left(\frac{(x_{ij} - x_{kj})^2}{(x_{\mathrm{M}j} - x_{\mathrm{m}j})^2} \delta^j_{ik} \right) \quad (1)$$

where x_{ij} represents the value of proxy j at year i, x_{kj} corresponds to the value of proxy j at year k, M and m refer to the maximum and minimum value of the proxy j. δ^j_{ik} is an index equal to 1 if a value is available for proxy j at year i and k, and equals 0 otherwise.

In the present paper, the AM was first used to infill both proxy and PDSI matrix (Fig. 2 [1]). Since most available tree rings series terminated before ~1993 (Table 1), we chose not to infill the proxy matrix up to the present, in order to reduce the possible

CPD
7, 153–198, 2011

bias associated with the use of an infilling method during the calibration period. Additionally, Dai et al. (2004)'s PDSI dataset presented some irregularities (in both mean and variance) before ~1930 in SSA. These irregularities are most likely associated with the very low number and poor quality of temperature and precipitation records in the early 20th century in that area. We therefore defined the 1930–1993 period for calibration. 101 PDSI series were retrieved from Dai et al. (2004)'s dataset. We selected the first 12 PC explaining 77% of the variance of the original PDSI series (Fig. 2 [2]).

2.4 Spectral analogue method (SAM)

The reconstruction of the 12 PC of PDSI is also based on the AM, but it is performed separately for each frequency band using a spectral analogue method (SAM). The SAM (Guiot et al., 2010) is a combination of the AM with a spectral decomposition procedure that aims at achieving the reconstruction separately for each frequency band (HF=high frequency band, LF=low frequency band). We defined the LF band as all periodicities below $f=0.08$ (or $T<12$ years, fixed by experimentation) and the HF band as all periodicities between 0.08 and 0.5 (12 years$>T>$2 years). While it is assumed that all frequency bands are present in the PDSI series ($0<f<0.5$), the SAM method allowed to choose, for each frequency, which proxies are the most reliable predictors. The decomposition of both proxy and PDSI series into their LF and HF component is achieved through a spectral decomposition algorithm (SD, Fig. 2 [3]) based on the Fast Fourier Transform (FFT). The FFT first transforms each series into the frequency domain. Then, all frequencies within the band (either LF or HF) are set to zero. Finally, the resulting spectrum is back-transformed into the time domain using the inverse FFT. The two bands are thus complementary because their summation restitutes the original series. For each frequency component, the AM is used to reconstruct the corresponding band of the PDSI PCs over the last millennia (Fig. 2 [4]). Once each frequency band is reconstructed independently, the series are restituted (SR) and back-transformed into the original gridded PDSI data using an inverse PC (PC^{-1}) procedure (Fig. 2 [5,6]).

CPD
7, 153–198, 2011

2.5 Uncertainty assessment

In the present paper, steps 4 to 6 on Fig. 2 are repeated iteratively (100 times here) and allowed for the implementation of an *h*-block jackknife procedure (Guiot et al., 2010) that enabled for the calculation of validation statistics and the computation of confidence intervals around reconstructed values. At each iteration, a year t is removed from each frequency band, along with the four preceding and following years (h=9) The AM is then used to predict the left-out year t from the training dataset in each band. This particular procedure aims at excluding, as potential analogues of year t, the years that are located immediately before or after the left-out year. This adaptation of the traditional jackknife method has proven to be particularly useful with series (like LF series) that present a high degree of autocorrelation (Guiot et al., 2010). In other words, it reduces the chances that the best analogue for year t, is found at year ($t-4$ to $t+4$). An analysis of the autocorrelation structure within summer PDSI series reveals that the years located immediately outside the block have less than 30% of variance in common with year t. Such a procedure, performed iteratively with a different (randomly chosen) year excluded at each time, enabled the calculation of the RE (Reduction of Error) a common validation statistic (Fig. 2 [7]) that is frequently used in dendroclimatology (Fritts, 1976). Moreover, the information produced at each iteration allowed for the computation of 95% confidence intervals around calibration statistics such as R (correlation coefficient) and R^2 (coefficient of determination).

As a further validation for our reconstructions, we used a published sedimentological record of Mar Chiquita's lake levels fluctuations (Piovano et al., 2002). Mar Chiquita is a large Sub-Tropical lake (about 6000 km^2 in size) that drains a vast area (about 127 000 km^2). It is reasonable to assume that the fluctuations of such a vast hydrosystem are controlled by parameters (temperature and precipitation) that are similar to those that also influence summer PDSI in the area. Thus, this record might be adequate to evaluate the quality of our reconstruction, at least the long-term trends.

CPD
7, 153–198, 2011

3 Results and discussion

3.1 Calibration and validation statistics of the SAM

The SAM yields satisfying results and suggests that the PDSI can be reconstructed in most areas of SSA. A good fit exists between observations and predictions for the full calibration period (1930–1993) (Fig. 3), and this fit is reasonably good in each frequency band (Fig. 4). The mean R for SSA is 0.65 and ranges from 0.48 (5th percentile) to 0.76 (95th percentile) (Table 2) for the full spectra. The average correlation coefficient is also very similar between the studied regions, with the lowest R value found in PM (0.62) and the highest in the PG region (0.68). In average, the SAM reconstructs about 40% of the variance of the PDSI in SSA (Table 2). The explained variance varied between 20% and 60%. Figure 5 shows the spatial distribution of these calibration statistics. In general, the relationships between observations and predictions tend to be slightly weaker in the easternmost part of SSA and the southern part of the Andes, probably as a consequence of the smaller density of proxy series in this area, especially low frequency proxies. Another possibility is that the PDSI itself might be less well estimated in this region of high climatological variability and altitudinal contrasts.

A property of the spectral analogues method, by comparison to other reconstruction methods that are based, for example, on multiple regression analysis, is to preserve a large amount of the original variance within the series. In other words, when a regression technique is used, the proportion of reconstructed variance decreases with the R^2. This attenuation effect becomes even more exaggerated in the past because the number of proxies diminishes with time. Spectral analogues, on the other side, are less sensitive to these effects since they are similarity-based and consequently they are able to reproduce a large part of the variance contained in the original series. To illustrate this effect in SSA, we calculated the ratio of standard deviations between reconstructed and observed PDSI series in each region and observed that the former

CPD
7, 153–198, 2011

corresponds to about 85 to 95% of the latter. Therefore, we conclude that this property facilitates the analysis of extremes. However, it is counterbalanced by the fact that the SAM does not have the capacity to extrapolate over the observed variability. Our reconstruction must therefore be seen as a conservative one.

Validation statistics confirm the predictive skills of our model. The RE statistic is almost exclusively positive over SSA (Table 2), suggesting that the spectral analogues provide better estimates of the PDSI than the mean PDSI value calculated on the calibration period. The mean RE value was, in average, greater than 0.30 in all subregions except the ANDES (0.20) but generally oscillated between 0 and 0.52 (95% percentiles over all SSA). These performances are comparable to the RE values obtained with the same method applied in Europe to reconstruct growing season temperatures (Guiot et al., 2010) and slightly below the average RE (0.6) obtained by Neukom et al. (2010a) in a principal component reconstruction of DJF temperatures in SSA. However, RE statistics are comparable to those found in the precipitation reconstruction (average RE over 0.27 in both seasons, Neukom et al., 2010b). Our RE values in the Mediterranean region of the Andes (about 0.35) are nevertheless comparable to the RE calculated by Christie et al. (2009) in a tree-ring reconstruction of PDSI in this area (∼0.45). However, Christie et al. (2009)'s reconstruction focused on high frequencies, while our multi-proxy reconstruction aims at reconstructing the full spectra of PDSI variations. Therefore, the comparison between RE statistics should be interpreted with care, as errors propagate differently when HF and LF bands are reconstructed simultaneously.

Another indication of the performance and usefulness of the SAM is that it is able to reproduce the spatial patterns of variations of the PDSI in SSA. Figure 6 presents the maps of the average observed and reconstructed PDSI values for two consecutive ∼30-year time windows (1931–1961 and 1961–1993). The first period (1931–1961) is marked by wet conditions in PG and the ANDES and a dryer climate in PA and ST. This pattern is very clearly seen in our reconstruction. The second period (1961–1993) has the opposite configuration; a wet climate in PM and ST and dryer conditions

CPD
7, 153–198, 2011

in PG and the ANDES. This spatial inversion of PDSI trends was well captured in our reconstruction.

As an independent validation, we checked the correspondence between our reconstruction and the 1767–2002 reconstruction of laguna Mar Chiquita water-levels fluctuation (Piovano et al., 2002). We used the average PDSI within the lake's watershed as a comparison (60–65° W; 20–25° S). The agreement between the two series is fairly good (Fig. 7), at least in the mid to low frequency domains, considering that both reconstructions were performed from totally independent proxies. A certain lag exists between the two reconstructions and that probably results from the imprecise dating of lake sediments. The abrupt rise of Mar Chiquita's lake levels during the 1970s also corresponds to a rise in PDSI, although the latter has a smaller amplitude. Two possibilities must be envisaged. A recent modeling of mar Chiquita's water-levels has shown that the recent rise is attributable to an increase in runoff in the northern sub-basin (Troin et al., 2010) evoking an increasingly dominant tropical influence in the area. Thus, since the PDSI is a value that is standardized to reflect departures from local mean conditions, the average PDSI within the mar Chiquita watershed may not adequately reflect this possible flow redistribution. The second relates to the fact that the recent rise is somewhat exaggerated by the increase of anthropic activities in the watershed (irrigation and agriculture and massive deforestation).

3.2 PDSI fluctuations over the last millennia in SSA

Figure 8 presents the PDSI reconstructions for the A.D. 1000–2005 period. PG's climate has alternated between relatively dry (1000–1250, 1480–1780, 1960–1990) and wet (1750–1900) periods (Fig. 8). Between ~1250 and ~1480, the PDSI fluctuated around zero, indicating conditions similar to the present. By contrast with PG, PM experienced wetter conditions between 1000 and 1250 while the period between 1250 and 1480 was generally dryer (Fig. 8). Another dry period was identified between 1780 and 1880 (Fig. 8). From about 1880, the climate of PM became increasingly wet to reach PDSI extremes (2002 and 2003, PDSI=5.78 and 5.4, respectively) that

CPD
7, 153–198, 2011

were never equaled in magnitude over the last thousand years. PDSI fluctuations in ST and the ANDES were generally similar to those of PM with a clear wet period between 1000 and ∼1250 and dry conditions that persisted until ∼1470 in ST and until about 1400 in the ANDES (Fig. 8). Afterwards, the climate became wetter in both ST and the ANDES. Over the last decades, both regions have experienced increasingly dry conditions. SSA, taken as a whole, experienced more moderate PDSI variations over the last millennia (Fig. 8). However, a wet period can be clearly identified prior to ∼1250. Then, the climate shifted to dryer conditions between ∼1250 and 1400, fluctuated around PDSI=0 between ∼1600 and ∼1800 and became increasingly wet during the middle of the 19th century. Ultimately, the climate dried up during the last century in SSA.

A striking feature of these reconstructions is that long-term PDSI variations in PG are clearly in antiphase with those found on the rest of the subcontinent. The analysis of long-term PDSI fluctuations is presented on Fig. 9 and was performed by smoothing each reconstruction individually with a low pass (50 years) filter. This analysis reveals that, at least at the secular scale, SSA's summer PDSI evolution, rather then being uniform over all the studied area, was characterized by an important geographical contrast, especially between the northeast and the southernmost part of the continent. That contrast can be most easily perceived in the low frequency domain (f <0.03), but it characterizes, typically, all frequency bands below 0.2 (T =5 years).

To highlight the significance and synchronicity of these changes in all regions, we performed a regime shift detection analysis. We used the procedure given by Rodionov et al. (2004) in order to detect the breakpoints in the PDSI's mean. Forcing the breakpoints to be at least of 50 years in length, the analysis revealed multiple regimes shifts in the series. The detailed analysis of changepoints highlighted the fact that the period between 1000 and ∼1250 was clearly a distinct regime in all areas (Fig. 10). Breakpoints corresponding to the end of the latter period were identified in 1242 (ST), 1244 (PM), ST (1270), 1237 (ANDES and SSA). This period corresponds to the end of the Medieval Warm Period (MWP) that extended until 1200–1350 in the

CPD
7, 153–198, 2011

Northern Hemisphere (Jansen et al., 2007; Mann et al., 2009; Guiot et al., 2005, 2010; DahlJensen et al., 1998), and until about 1200–1250 in the Southern Hemisphere (Cook et al., 2002). In SSA, the MWP seemed to have persisted until about 1400 (Neukom et al., 2010a). The 150-year lag between our PDSI reconstruction and Neukom et al.'s (2010a) summer temperature reconstruction need further investigation but could possibly be explained by changes in precipitation patterns that are not seized by temperature reconstructions. It is interesting to note however that, from the perspective of PDSI, the MWP in SSA was probably a period of important geographical contrasts rather than a widespread drought. Our findings nevertheless support the idea that the MWP was probably a global phenomena (Broecker, 2001), but its expression, from the point of view of water availability might have been considerably contrasted between regions.

In order to make sure that the 1000–~1250 period is not simply a statistical artifact caused by the lower number of proxies covering that period (Fig. 1), we performed alternative reconstructions using exclusively the proxies that extend beyond AD. 1250 in the past (Fig. 11). The results show that the even with a limited number of proxies that cover the full millennia, the 1000–~1250 period can still be clearly identified. More particularly, our analysis shows that LFs are comparable between reconstructions over the last thousand years. However, the HFs are less similar and this probably relates to the fact that higher frequencies contain a lot of the local climatic signal (i.e noise) that cannot be adequately reconstructed from a very limited number of HF proxies. Nevertheless, the correlations for the full spectra remain acceptable, suggesting that the long-term trends can be interpreted over the full reconstruction period.

The 1250–1380 period is clearly distinct in all regions of SSA and is characterized by generally dry conditions (Fig. 10), except in PG where wetter than average conditions prevailed. Interestingly, this well-defined regime corresponds to the Wolf glacial Minima (Eddy, 1976), the first period of extremely low sunspot activity of the LIA, occurring immediately after the MWP. This period is not visible in Neukom et al. (2010a)'s reconstruction of summer temperature for SSA and therefore we hypothesize that it

CPD
7, 153–198, 2011

must reflect a precipitation-induced rather than a temperature-induced regime change. Afterwards, regimes wetter than the normal were identified between 1375 and 1553 in PM and between 1471 and 1756 in ST, respectively during the Spörer and the Maunder Minima (Eddy, 1976). The physical links between solar irradiation and the PDSI in SSA need to be substantiated by further modeling studies in order to clarify the processes and forcings involved.

Although important regime changes occurred over the last centuries, most of those identified fell within the bounds of the last millennia's variability (Fig. 10). The best example is the drying episode that occurred in PG since 1880. Similar regime conditions could be found between 1400 and 1750 in the area, and even before ~1250. However, some exceptions must be underlined. In PM, the recent trend towards wetter conditions is clearly exceptional at the scale of the last millennia; as is the drying trend observed in the ANDES since the 1930s that has no equivalent in the past whatsoever (Fig. 10).

An analysis of extremes allowed to describe past PDSI values corresponding to design events such as the 100-year drought and wet spell over the last millennia. To perform this analysis, we iteratively identified, for each year t and for each region, the corresponding percentiles (0.01 for droughts and 0.99 for wet spells) from a set of 50 years randomly drawn within the 100 preceding years. The results, plotted with their 95% confidence intervals, are depicted on Fig. 12. The last 250 years were exceptional regarding the behaviour of extremes. In PG, the PDSI value of the 100-year wet spell has been systematically over 2 during the last 250 years (Fig. 12). This value was never equaled in magnitude over the last millennia. In PM, the 100-year wet spell reached a PDSI value superior to 4 after 1990 and that also is exceptional at the time scale investigated (Fig. 12). The last 250 years in ST were characterized by 100-year wet spells that were superior to 2, a value that was exceeded only during the MWP (Fig. 12). Intriguingly, in this area, extreme 100-year droughts also became more severe, reaching −2 in average, and therefore highlighting the important variability during that recent period. Finally, despite a clear and prolonged increasing tendency in the

CPD
7, 153–198, 2011

PDSI value of the 100-year wet spell, the recent dry episode in the ANDES is exceptional at the scale of the last millennia (Fig. 12). At the scale of SSA, the PDSI values of the 100-year wet spells and droughts were relatively high during the MWP, decreased abruptly around 1250 and slowly increased afterwards (Fig. 12). Extreme 100-year droughts became more severe during the last century in SSA (Fig. 12).

3.3 Links with ocean-atmosphere forcings (AAO, ENSO, PDO)

The climate of SSA is under the influence of high latitude and tropical ocean-atmosphere forcings, but the magnitude and the direction of this influence varies considerably between regions. To explore the teleconnections between summer PDSI and the dominant indices in the area (summer means for AAO, ENSO, PDO), we first used standard Pearson correlation analysis. Reconstructed PDSI values were used as predictands, but we also tested the relationships with instrumental PDSI values and the results are comparable (see Fig. A2, for a comparison). This allowed to demonstrate that our reconstructions have a physical meaning and that they are able to reproduce the climatic pattern driven by the major indices in SSA. By contrast with Christie et al. (2009)'s regional reconstruction, the correlations were not performed on prewhitened series (PDSI and atmospheric indexes) because it is thought that the persistence found in both predictand and predictor series are usefull climatic information that should not be removed. The AAO index is estimated by the first PC of the 850 hPa geopotential height anomalies south of 20° S. The ENSO index corresponds to the mean SST anomalies from the N3.4 Pacific region and is a common proxy for the ENSO phenomena. Finally, the PDO is an ENSO-like phenomena that exhibits decadal to interdecadal variability (at least 20 to 30 years). However, the estimation of the PDO's interdecadal variability remains poorly known because very few stations in South-America are century-long.

Over the common period (1949–2005), AAO is well correlated to summer PDSI in SSA. In PG and the ANDES, the correlation is negative and reaches $r=-0.53$ while in PM and ST, the correlation is positive (Fig. 13) and reaches $r=0.5$. Thus, over the

CPD
7, 153–198, 2011

last 50 years, AAO fluctuations have been associated with important climatic contrasts in SSA. Positive AAO indices are clearly associated with wet conditions in western PM and ST and with dry conditions in PG and the ANDES (Fig. 13). Negative AAO values show the opposite trend: wet PG and dry PM/ST (Fig. 13). This latitudinally contrasted response of summer PDSI to the AAO might have some important implications for the interpretation of millennial PDSI trends in SSA. We showed earlier (Fig. 9) that low-frequency variations of summer PDSI in the southernmost part of SSA have been in antiphase with those on the rest of the sub-continent. It is now possible to argue that these antiphases could have been driven by past low-frequency variations in the AAO. The AAO is the leading pattern of tropospheric circulation variability south of 20° S (Garreaud et al., 2009). Its influence on temperature and precipitation over the recent period is unequivocal over the recent period (Gillett et al., 2006; Garreaud et al., 2009). The most striking aspect is a contrasted response of surface temperatures with a clear warming south of 40° S and a cooling elsewhere during positive phase of the AAO (Garreaud et al., 2009). These results highlight the fact that summer PDSI variations in SSA are responsive to AAO-induced temperature fluctuations at the continental scale.

Summer PDSI is also related to the ENSO phenomena in SSA (1951–2005). However, the relationship is far less contrasted than with AAO and mostly positive throughout the studied area (Fig. 13). The strongest correlations are found in the Mediterranean area of the Andes and along the eastern coast of Argentina. Positive (negative) ENSO years typically generate conditions that are wetter (dryer) that the normal in SSA (Fig. 13). PDO is more discretely related to the fluctuations of summer PDSI (1930–2005). This index has a general positive influence, but the highest correlations (r=0.5) are found in the Mediterranean Andes region (Fig. 13). Much like with ENSO, positive (negative) PDO years generate conditions that are wetter (dryer) that the normal almost everywhere SSA, except in PG (Fig. 13)

However, to determine, for each region, which atmospheric index has a predominant influence on summer PDSI over the 1950–2005 period, we performed a regression analysis using each index as a predictor. For each 2.5°×2.5° pixel in SSA, the equation

CPD
7, 153–198, 2011

had the form PDSI=a(AAO)+b(ENSO)+c(PDO)+noise, where a, b, c are coefficients. For each regression, we retained the largest coefficient (absolute value) and noted its sign. Figure 14 plots these coefficients. Interestingly, this figure clearly shows that the various sub-regions of SSA are under the influence of different dominant indexes. In PG and northeastern ST, the dominant process is clearly the negative and spatially coherent influence of AAO on summer PDSI. A positive influence of AAO is also dominant west of 70° W in PM and in lower ST. Both PDO and ENSO are most influential in the Mediterranean ANDES, in western PM and in ST.

The spatialization of these influences is crucial for an adequate understanding of past PDSI variations in SSA. However, it is must be clear from our results that all these processes act synergically rather than isolately in order to modulate SSA's climate and PDSI variations. Moreover, the influence of each of these processes might be very strong in some periods (or regions), and weaker in others (Garreaud et al., 2009). To illustrate this phenomena, we performed a continuous wavelet transform (cwt) in an attempt to identify the most important periodicities in each PDSI series (Fig. 15). More particularly, we performed this analysis in order to identify the 2–8 years periodicities that could correspond to ENSO-like phenomena, and the low frequency >10 years periodicities possibly associated with an AAO forcing. This analysis revealed that, in all series, the low frequency band (>30 years) is a dominant component. In PG and PM, (Fig. 15), the low frequencies dominate, but an important part of the variance can also be found on smaller ENSO-like periodicities, especially between 1450 and 1750. The range of significant periodicities is large after ~1750, and this should be put in relation with the fact that climate, in that area, recently became much more variable at all time scales. Interestingly, in ST, ENSO-related periodicities are very weak and most of the variance is related to low frequency variations (Fig. 15). By contrast, in the ANDES, ENSO-like periodicities are omnipresent. They are at their strongest between 1000 and 1250, and between 1450 and 1750, while very low frequencies are much less important than in the other regions (Fig. 15). Ultimately, spectral properties of SSA, taken as a whole, reveal that, at the sub-continental scale, low frequencies are dominant and

CPD
7, 153–198, 2011

that ENSO-like periodicities exist, but are of lesser importance (Fig. 15). Thus, the latter analysis describes a complex imbrication of periodicities and suggests that multiple processes acting at various time-scales possibly influence long-term variations of PDSI in SSA. It clearly shows that although low frequency periodicities generally dominate in SSA (those are probably AAO-related), other periodicities observable on higher frequency bands have been important (if not dominant) contextually. In other words, PDSI variations over the last millennia in SSA cannot be associated to a single and dominant index, but to a combination of many indexes whose interdependence over the last millennia is not yet fully understood. More research is therefore required to precise the interconnections between these ocean-atmosphere forcings and to better document their impacts on long term PDSI fluctuations in SSA.

4 Conclusions

This study presents the first spatially and temporally highly resolved summer PDSI reconstruction in the Southern Hemisphere. We provide a 2.5×2.5° gridded reconstruction that extends the Dai et al. (2004) PDSI dataset over the last millennia at the sub-continental scale, south of 20° S in SSA. Calibration and verification statistics, along with the spatial analysis of modern patterns of changes show that, in most areas of SSA (PG, PM, ST, ANDES), the summer PDSI is well reconstructed using the SAM. The latter method aims at recreating the full spectrum of variations of the PDSI by reconstructing the lower frequencies independently from the higher ones.

Over the last millennia, SSA has experienced considerable PDSI variations, some of which might have been more important than those recently observed in the area. The temporally well-defined 1000–1250 period possibly associated with the MWP was characterized by wetter than normal conditions in most studied regions except in PG where the climate was clearly drier that the normal. This regime terminated very abruptly around ~1250, as indicated by the regime shift detection and the analysis of extremes.

CPD
7, 153–198, 2011

In most regions, the climatic configuration reversed between 1250 and ∼1400. SSA's climate became much drier, except in PG where the climate humidified during the austral summer. Afterwards, SSA slowly humidified to approach conditions somewhat closer to the normal (although with some important discrepancies between regions). The analysis of recent fluctuations in the context of the last millennia reveals that, although rare, analogues of the modern period exist in the past, especially between 1000 and 1400. However, the recent trend towards increasingly moist conditions observed in PM was found to be exceptional, both in terms of regime and extremes, over the last thousand years. We reach a similar conclusion concerning the recent droughts in the ANDES.

Our reconstructions also show that PG's fluctuations were generally in antiphase with the rest of the continent. Our analysis suggest that these antiphases could be driven by the Antarctic Oscillation (AAO). We provide evidences that the AAO has contrasted effects on the PDSI in SSA over the calibration period. During its positive phase, the climate tends to be humid in the northeastern part of SSA and much drier in the south. During its negative phase, the latter situation reverses. Thus, we believe that, if the relationship between AAO and summer PDSI holds for the past and was stationary through time (which is implicitly hypothesized in all reconstruction models), then AAO might have been an important climatic driver over the last millennia, at least in the low frequency domain. However, AAO has probably never act alone to modulate fluctuations in the mean and extremes of PDSI. In some regions like PG, AAO has clearly been the dominant driver (at least during the calibration period) while in others in has played a smaller role. However, we must also highlight the fact that processes such as ENSO and PDO have also introduced high frequency variations in SSA's summer PDSI, with the strongest ENSO-like periodicites found in PG, PM and the ANDES during the 1400–1750 period when low frequency variations were less important in most series. It would therefore be important that future analysis focus on studying the interactions between ocean-atmosphere indices in order to better precise how they can modulate SSA's climate in both time and space. Such work should preferentially

CPD
7, 153–198, 2011

be achieved using climate models, but our reconstruction could certainly be used as a gauge for detection and attribution studies.

Appendix A

Complementary figures

Figure A1 represents the Goethite (derivative 445 nm) varved chronology of Lago Frias sediments (1645–2008). This sedimentary proxy reflects the amount of precipitation-induced erosion in the watershed. The dating of these sediments was confirmed by three well-known earthquakes (1737, 1751 and 1960) also shown on the figure. Figure A2 represents de correlation between AAO, ENSO and PDO and Dai et al. (2004)s original gridded PDSI data. We present these maps in appendix in order to show that the patterns of correlation are very similar to those reconstructed using the SAM method (see Fig. 13), therefore reinforcing the fact that our method reproduces well the most important large scale climatic patterns in SSA.

Acknowledgements. This paper is a contribution to the ESCARSEL project funded by the French National Agency of Research (program VMC, project ANR-06-VULN-010). We also thank the post-doctoral fellowship program of the FQRNT (Fonds Québécois de Recherche sur la Nature et les Technologies) that provided the grant to the first author. Francoise Chalié, Edouardo Piovano Francoise Vimeux, Florence Sylvestre, Raphael Neukom that provided data and/or helpful discussions.

CPD
7, 153–198, 2011

The publication of this article is financed by CNRS-INSU.

References

Apipattanavis, S., McCabe, G. J., Rajagopalan, B., and Gangopadhyay, S.: Joint spatiotemporal variability of global sea surface temperatures and global Palmer Drought Severity Index values, J. Climate, 22, doi:10.1175/2009JCLI2791.1171, 6251–6267, 2009.

Ariztegui, D., Bosch, P., and Davaud, E.: Dominant ENSO frequencies during the Little Ice Age in Northern Patagonia: the varved record of proglacial Lago Frias, Argentina, Quatern. Int., 161, 46–55, doi:10.1016/J.Quaint.2006.10.022, 2007.

Black, D. E., Abahazi, M. A., Thunell, R. C., Kaplan, A., Tappa, E. J., and Peterson, L. C.: An 8-century tropical Atlantic SST record from the Cariaco Basin: baseline variability, twentieth-century warming, and Atlantic hurricane frequency, Paleoceanography, 22, PA4204 doi:10.1029/2007PA001427, 2007.

Boninsegna, J. A., Villalba, R., Amarilla, L., and Ocampo, J.: Studies on tree rings, growth-rates and age-size relationships of tropical tree species in Misiones, Argentina, Iawa Bull., 10, 161–169, 1989.

Bradley, R. S. and Jones, P. D.: "Little Ice Age" summer temperature variations: their nature and relevance to recent global warming trends, Holocene, 3, 367–376, 1993.

Briffa, K. R., Osborn, T. J., Schweingruber, F. H., Jones, P. D., Shiyatov, S. G., and Vaganov, E. A.: Tree-ring width and density data around the Northern Hemisphere: Part 1, local and regional climate signals, Holocene, 12, 737–757, 2002.

Broecker, W. S.: Paleoclimate – was the medieval warm period global?, Science, 291, 1497–1499, 2001.

Christie, D. A., Boninsegna, J. A., Cleaveland, M. K., Lara, A., Le Quesne, C., Morales, M. S., Mudelsee, M., Stahle, D. W., and Villalba, R.: Aridity changes in the Temperate-Mediterra-

nean transition of the Andes since AD 1346 reconstructed from tree-rings, Clim. Dynam., doi:10.1007/s00382-009-0723-4, 2009.
Cook, E. R., Meko, D. M., Stahle, D. W., and Cleaveland, M. K.: Drought reconstructions for the continental United States, J. Climate, 12, 1145–1162, 1999.
Cook, E. R., Palmer, J. G., and D'Arrigo, R. D.: Evidence for a Medieval Warm Period in a 1100 year tree-ring reconstruction of past austral summer temperatures in New Zealand, Geophys. Res. Lett., 29, 1667, doi:10.1029/2001gl014580, 2002.
Cook, E. R., Woodhouse, C. A., Eakin, C. M., Meko, D. M., and Stahle, D. W.: Long-term aridity changes in the Western United States, Science, 306, 1015–1018, doi:10.1126/science.1102586, 2004.
DahlJensen, D., Mosegaard, K., Gundestrup, N., Clow, G. D., Johnsen, S. J., Hansen, A. W., and Balling, N.: Past temperatures directly from the Greenland Ice Sheet, Science, 282, 268–271, 1998.
Dai, A., Trenberth, K. E., and Quian, T.: A global dataset of Palmer Drought Severity Index for 1870–2002: relationship with soil moisture and effects of surface warming, J. Hydrometeorol, 5, 1117–1130, 2004.
Eddy, J. A.: Maunder minimum, Science, 192, 1189–1202, 1976.
Esper, J., Cook, E. R., and Schweingruber, F. H.: Low-frequency signals in long tree-ring chronologies for reconstructing past temperature variability, Science, 295, 2250–2253, 2002.
Esper, J., Frank, D. C., and Wilson, R. J. S.: Climate reconstructions: low-frequency ambition and high-frequency ratification, Eos, 85, p. 113, 2004.
Fritts, H. C.: Tree Rings and Climate, Academic Press, New York, 1976.
Garreaud, R. D.: Precipitation and circulation covariability in the extratropics, J. Climate, 20, 4789–4797, doi:10.1175/Jcli4257.1, 2007.
Garreaud, R. D., Vuille, M., Compagnucci, R., and Marengo, J.: Present-day South American climate, Palaeogeogr. Palaeocl., 281, 180–195, 2009.
Gillett, N. P., Kell, T. D., and Jones, P. D.: Regional climate impacts of the southern annular mode, Geophys. Res. Lett., 33, L23704, doi:10.1029/2006gl027721, 2006.
Goosse, H., Masson-Delmotte, V., Renssen, H., Delmotte, M., Fichefet, T., Morgan, V., van Ommen, T., Khim, B. K., and Stenni, B.: A late medieval warm period in the Southern Ocean as a delayed response to external forcing?, Geophys. Res. Lett., 31, L06203, doi:10.1029/2003gl019140, 2004.
Guiot, J., Nicault, A., Rathgeber, C., Edouard, J. L., Guibal, F., Pichard, G., and Till, C.:

CPD
7, 153–198, 2011

Last-millennium summer-temperature variations in Western Europe based on proxy data, Holocene, 15, 489–500, 2005.
Guiot, J., Corona, C., and Escarsel, M.: Growing season temperatures in Europe and climate forcings over the past 1400 years, Plos Biol, 5, e9972, doi:10.1371/journal.pone.0009972, 2010.
von Gunten, L., Grosjean, M., Rein, B., Urrutia, R., and Appleby, P.: A quantitative high resolution summer temperature reconstruction based on sedimentary pigments from Laguna Aculeo, Central Chile, back to AD 850, Holocene, 19, 873–881, 2009.
Haberzettl, T., Fey, M., Lucke, A., Maidana, N., Mayr, C., Ohlendorf, C., Schabitz, F., Schleser, G. H., Wille, M., and Zolitschka, B.: Climatically induced lake level changes during the last two millennia as reflected in sediments of Laguna Potrok Aike, Southern Patagonia (Santa Cruz, Argentina), J. Paleolimnol., 33, 283–302, doi:10.1007/S10933-004-5331-Z, 2005.
Jansen, E., Overpeck, J., Briffa, K. R., Duplessy, J. C., Joos, F., Masson-Delmotte, V., Olago, D., Otto-Bliesner, B., Peltier, W. R., Rahmstorf, S., Ramesh, R., Raynaud, D., Rind, D., Solomina, O., Villalba, R., and Zhang, D.: Palaeoclimate, in: Climate Change 2007: The Physical Science Basis, Contribution of Working Group I to the Fourth Assessment Report of the Intergovernmental Panel on Climate Change, edited by: Solomon, S., Qin, D., Manning, M., Chen, Z., Marquis, M., Averyt, B., Tignor, M., and Miller, H. L., UK and New York, NY, USA, 2007.
Jones, P. D., Briffa, K., Barnett, T. P., and Tett, S. F. B.: High-resolution palaeoclimatic records for the last millennium: interpretation, integration and comparison with general circulation model control-run temperatures, Holocene, 8, 455–471, 1998.
LaMarche, V. C., Holmes, R. L., Dunwiddie, P. W., and Drew, L. G.: Argentina and Chile, in: Tree-Ring Chronologies of the Southern Hemisphere, Vol. 12, University of Arizona, Tuscon, Arizona, USA, 1979.
Lara, A., Villalba, R., and Aravena, J. C.: Desarollo de una red de cronologias de Fitzroya cupressoides (Alere) para Chile y Argentina, in: Dendrochronologia en America Latina, edited by: Roig, F., Mendoza, Universidad Nacional de Cuyo, Mendoza, Argentina, 217–244, 2000.
Magrin, G., Gay García, C., Cruz Choque, D., Giménez, J. C., Moreno, A. R., Nagy, G. J., Nobre, C., and Villamizar, A.: Latin America, in: Climate Change 2007: Impacts, Adaptation and Vulnerability, Contribution of Working Group II to the Fourth Assessment Report of the Intergovernmental Panel on Climate Change, edited by: Parry, M. L., Canziani, O. F., Palu-

CPD
7, 153–198, 2011

tikof, J. P., van der Linden, P. J., and Hanson, C. E., Cambridge University Press, Cambridge, 581–615, 2007.
Mann, M. E., Bradley, R. S., and Hughes, M. K.: Global-scale temperature patterns and climate forcing over the past six centuries, Nature, 392, 779–787, 1998.
Mann, M. E., Bradley, R. S., and Hughes, M. K.: Northern Hemisphere temperatures during the past millennium: inferences, uncertainties, and limitations, Geophys. Res. Lett., 26, 759–762, 1999.
Mann, M. E., Zhang, Z. H., Rutherford, S., Bradley, R. S., Hughes, M. K., Shindell, D., Ammann, C., Faluvegi, G., and Ni, F. B.: Global signatures and dynamical origins of the Little Ice Age and medieval climate anomaly, Science, 326, 1256–1260, doi:10.1126/Science.1177303, 2009.
Moberg, A., Sonechkin, D. M., Holmgren, K., Datsenko, N. M., and Karlen, W.: Highly variable Northern Hemisphere temperatures reconstructed from low- and high-resolution proxy data, Nature, 433, 613–617, doi:10.1038/Nature03265, 2005.
Neukom, R., Luterbacher, J., Villalba, R., Küttel, M., Frank, D., Jones, P., Grosjean, M., Wanner, H., Aravena, J.-C., Black, D., Christie, D., D'Arrigo, R., Lara, A., Morales, M., Soliz-Gamboa, C., Srur, A., Urrutia, R., and von Gunten, L.: Multiproxy summer and winter surface air temperature field reconstructions for Southern South America covering the past centuries, Clim. Dynam., doi:10.1007/s00382-00010-00793-00383, 2010a.
Neukom, R., Luterbacher, J., Villalba, R., Kuttel, M., Frank, D., Jones, P. D., Grosjean, M., Esper, J., Lopez, L., and Wanner, H.: Multi-centennial summer and winter precipitation variability in Southern South America, Geophys. Res. Lett., 37, L14708, doi:10.1029/2010gl043680, 2010b.
Nicault, A., Alleaume, S., Brewer, S., Carrer, M., Nola, P., and Guiot, J.: Mediterranean drought fluctuation during the last 500 years based on tree-ring data, Clim. Dynam., 31, 227–245, doi:10.1007/s00382-007-0349-3, 2008.
Palmer, W. C. : Meteorological drought. Research Paper No. 45, US Department of Commerce Weather Bureau, Washington, DC, 58 pp., 1965
Piovano, E. L., Ariztegui, D., and Moreira, S. D.: Recent environmental changes in Laguna Mar Chiquita (Central Argentina): a sedimentary model for a highly variable saline lake, Sedimentology, 49, 1371–1384, 2002.
Roig, F.: Dendrochronologia y dendroclimatologia del bosque de *Pilgerodendron uviferum* en su area norte de dispersion, Bol. Soc. Arg. Bot., 27, 217–234, 1991.

CPD
7, 153–198, 2011

Roig, F. A. and Boninsegna, J. A. : Chiloe Island summer precipitation constructed for 426 years from Pilgerodendron uviferum tree rings chronologies. Tree Rings and Environment: Proceedings of the International Dendrochronology Symposium: Lundqua report, 34, 277–280, 1992

Schmelter, A.: Climatic response and growth trends of Nothofagus pumilio along altitudinal gradients from arid to humid sites in Northern Patagonia, in: Dendrochronologia en America Latina, edited by: Roig, F., Mendoza, Universidad Nacional de Cuyo, Mendoza, Argentina, 193–215, 2000.

Trenberth, K. E., Jones, P. D., Ambenje, P., Bojariu, R., Easterling, D., Klein Tank, A., Parker, D., Rahimzadeh, F., Renwick, J. A., Rusticucci, M., Soden, B., and Zhai, P.: Climate Change 2007: The Physical Science Basis, Contribution of Working Group I to the Fourth Assessment Report of the Intergovernmental Panel on Climate Change, edited by: Solomon, S., Qin, D., Manning, M., Chen, Z., Marquis, M., Averyt, K. B., Tignor, M., and Miller, H. L., Cambridge, 2007.

Troin, M., Vallet-Coulomb, C., Sylvestre, F., and Piovano, E.: Hydrological modelling of a closed lake (Laguna Mar Chiquita, Argentina) in the context of the 20th century climatic changes, J. Hydrol., 393, 233–244, doi:10.1016/j.hydrol.2010.1008.1019, 2010.

Villalba, R., Holmes, R. L., and Boninsegna, J. A.: Spatial patterns of climate and tree growth variations in subtropical Northwestern Argentina, J. Biogeogr., 19, 631–649, 1992.

Villalba, R., Boninsegna, J. A., Veblen, T. T., Schmelter, A., and Rubulis, S.: Recent trends in tree-ring records from high elevation sites in the Andes of Northern Patagonia, Climatic Change, 36, 425–454, 1997.

Villalba, R. and Veblen, T. T.: Spatial and temporal variation in *Austrocedrus* growth along the forest – steppe ecotone in Northern Patagonia, Can. J. Forest Res., 27, 580–597 1997.

Vimeux, F., Ginot, P., Schwikowski, M., Vuille, M., Hoffmann, G., Thompson, L. G., and Schotterer, U.: Climate variability during the last 1000 years inferred from Andean ice cores: a review of methodology and recent results, Palaeogeogr. Palaeoecl., 281, 229–241, 2009.

Woodhouse, C. A. and Brown, P. M.: Tree-Ring evidence for great plains drought, Tree-Ring Res., 57, 89–103, 2001.

Woodhouse, C. A. and Overpeck, J. T.: 2000 years of drought variability in the Central United States, B. Am. Meteorol. Soc., 79, 2693–2714, 1998.

CPD
7, 153–198, 2011

Table 1. The proxies used to reconstruct summer PDSI in SSA. HF=proxies used to reconstruct the high frequency component ($0.08<f<0.5$). LF=proxies used to reconstruct the low frequency component ($0<f<0.08$).

Name	Type	SP	Start	End	Length	LAT	Long	Reference	HF	LF
Lago Yehuin	Tree rings	NOPU	1731	1986	255	54	67	Boninsegna et al. (1989)	X	
Pampa Del Toro	Tree rings	AUCH	1736	1991	255	41	71	Villalba and Veblen (1997)	X	
Angostura Lago Alumine	Tree rings	ARAR	1717	1974	257	38	71	LaMarche et al. (1979)	X	
Pilcaniyeu	Tree rings	AUCH	1733	1991	258	41	70	Villalba and Veblen (1997)	X	
Estancia Carmen Camino T. Del Fuego	Tree rings	NOPU	1726	1986	260	54	67	Boninsegna et al. (1989)	X	
Puerto Parry T. Del Fuego	Tree rings	NOBE	1726	1986	260	54	64	Boninsegna et al. (1989)	X	
Estancia San Justo,T Del Fuego	Tree rings	NOPU	1723	1985	262	54	68	Boninsegna et al. (1989)	X	
Confluencia 2	Tree rings	AUCH	1723	1989	266	37	71	Villalba and Veblen (1997)	X	
Bahia Crossley Isla De Los Estados	Tree rings	NOBE	1715	1986	271	54	65	Boninsegna et al. (1989)	X	
Paso De Las Nubes 3	Tree rings	NOPU	1718	1991	273	40	71	Villalba et al. (1997)	X	
Rio Kilca	Tree rings	ARAR	1700	1974	274	38	70	LaMarche et al. (1979)	X	
Laguna Terrapien	Tree rings	PIUV	1700	1974	274	43	71	LaMarche et al. (1979)	X	
Lago Rucachoroi	Tree rings	AUCH	1700	1974	274	39	71	LaMarche et al. (1979)	X	
Lago Terraplen	Tree rings	AUCH	1700	1974	274	43	71	Villalba and Veblen (1997)	X	
Buenos Aires, Santa Cruz	Tree rings	NOPU	1706	1984	278	50	72	ITRDB series arge066	X	
Rio Malenguena T. Del Fuego	Tree rings	NOPB	1705	1986	281	54	66	Boninsegna et al. (1989)	X	
El Maiten	Tree rings	PIUV	1690	1974	284	41	71	LaMarche et al. (1979)	X	
Estancia Harberton T. Del Fuego	Tree rings	NOBE	1700	1985	285	54	67	Boninsegna et al. (1989)	X	
Paso De Las Nubes 4	Tree rings	NOPU	1701	1991	290	40	71	Villalba et al. (1997)	X	
Rio Bolsas, Piedra Parada,Jujuy	Tree rings	JUAU	1688	1981	293	23	65	Villalba et al. (1992)	X	
Monte Grande, Magallanes	Tree rings	NOPU	1677	1988	311	53	72	ITRDB series arge049	X	
Volcan Lonquimay	Tree rings	ARAR	1664	1975	311	38	71	LaMarche et al. (1979)	X	
Paso Del Viento	Tree rings	AUCH	1679	1991	312	40	71	Villalba and Veblen (1997)	X	
Lago Quillèn	Tree rings	AUCH	1676	1989	313	39	71	Villalba and Veblen (1997)	X	
Aserradero Isla Grande T. Del Fuego	Tree rings	NOPB	1666	1986	320	54	67	Boninsegna et al. (1989)	X	
Estacion Microondas	Tree rings	NOPU	1664	1984	320	54	67	Boninsegna et al. (1989)	X	
Paso Gari Baldi	Tree rings	NOPB	1662	1985	323	54	71	Boninsegna et al. (1989)	X	
Lago Rucachoroi	Tree rings	ARAR	1650	1975	325	39	71	LaMarche et al. (1979)	X	
Peninsula Brunswick	Tree rings	NOPU	1662	1988	326	40	71	Boninsegna et al. (1989)	X	
El Chacay	Tree rings	AUCH	1650	1976	326	37	71	LaMarche et al. (1979)	X	
Copahue	Tree rings	ARAR	1640	1974	334	37	71	LaMarche et al. (1979)	X	
Paso Cordova, Neuquen	Tree rings	NOPU	1652	1986	334	40	71	ITRDB series arge050	X	
Lago Fontana, Chubut	Tree rings	NOPU	1647	1985	338	45	71	ITRDB series arge037	X	
Bahia York	Tree rings	NOBE	1647	1986	339	54	65	ITRDB series arge023	X	
Aserradero Isla Grande Monticulo	Tree rings	NOPB	1639	1986	347	54	67	Boninsegna et al. (1989)	X	
Castano Overo Maduro	Tree rings	NOPD	1626	1982	356	41	71	ITRDB series arge027	X	
El Mirador, Traful	Tree rings	AUCH	1635	1991	356	40	71	Villalba and Veblen (1997)	X	
Santa Isabel De Las Cruces	Tree rings	AUCH	1600	1970	370	34	70	LaMarche et al. (1979)	X	
Lago Moquehue	Tree rings	ARAR	1601	1974	373	38	71	LaMarche et al. (1979)	X	
Lago Tromen	Tree rings	ARAR	1600	1978	378	54	67	LaMarche et al. (1979)	X	
Glaciar Frias	Tree rings	NOPU	1595	1985	390	41	71	LaMarche et al. (1979)	X	
Estancia Collun-Co, Caòadon De Arriba	Tree rings	AUCH	1596	1989	393	39	71	Villalba and Veblen (1997)	X	
Estancia Pulmari	Tree rings	ARAR	1589	1989	400	39	71	LaMarche et al. (1979)	X	
Rio Minero	Tree rings	AUCH	1589	1991	402	40	71	Villalba and Veblen (1997)	X	
Lago Escondido	Tree rings	NOPB	1575	1984	409	54	67	Boninsegna et al. (1989)	X	
Castaòo Overo 8	Tree rings	NOPU	1572	1991	419	41	71	Villalba et al. (1997)	X	
Huinganco	Tree rings	AUCH	1550	1975	425	37	70	LaMarche et al. (1979)	X	
Nahuel – Pan	Tree rings	AUCH	1567	1992	425	42	71	Villalba and Veblen (1997)	X	
Norquinco	Tree rings	AUCH	1562	1989	427	39	71	Villalba and Veblen (1997)	X	

CPD
7, 153–198, 2011

Table 1. Continued.

Name	Type	SP	Start	End	Length	LAT	Long	Reference	HF	LF
Castaòo Overo 7	Tree rings	NOPU	1562	1991	429	41	71	Villalba et al. (1997)	X	
Cuyin Manzano	Tree rings	PIUV	1543	1974	431	40	71	LaMarche et al. (1979)	X	
Piuchue, Isla De Chiloe	Tree rings	PIUV	1554	1987	433	33	70	Roig (1991)	X	
Estancia Teresa	Tree rings	PIUV	1540	1974	434	42	71	LaMarche et al. (1979)	X	
Cerro Los Leones	Tree rings	PIUV	1539	1974	435	41	71	LaMarche et al. (1979)	X	
Cerro Diego De Leon	Tree rings	NOPU	1546	1991	445	41	71	Schmelter (2000)	X	
Castaòo Overo 6	Tree rings	NOPU	1539	1991	452	41	71	Villalba et al. (1997)	X	
Rio Moat T. Del Fuego	Tree rings	NOBE	1528	1986	458	54	66	Boninsegna et al. (1989)	X	
Cerro La Hormiga Estancia Collun-Co	Tree rings	AUCH	1508	1989	481	40	71	Villalba and Veblen (1997)	X	
Puente Del Agrio	Tree rings	ARAR	1486	1974	488	42	71	LaMarche et al. (1979)	X	
Rahue	Tree rings	PIUV	1483	1974	491	39	70	LaMarche et al. (1979)	X	
Cerro Del Guanaco	Tree rings	AUCH	1497	1991	494	41	70	Villalba and Veblen (1997)	X	
Lago Quillèn	Tree rings	AUCH	1508	2003	495	40	71	Villalba and Veblen (1997)	X	
Caramavida	Tree rings	ARAR	1479	1976	497	34	70	LaMarche et al. (1979)	X	
Santa Lucia, Chiloe Continental	Tree rings	PIUV	1489	1986	497	43	72	Roig and Boninsegna (1992)	X	
Santa Lucia	Tree rings	PIUV	1489	1986	497	43	72	Roig and Boninsegna (1992)	X	
El Centinela	Tree rings	AUCH	1491	1989	498	40	71	Villalba and Veblen (1997)	X	
Pino Hachado	Tree rings	PIUV	1459	1974	515	42	71	LaMarche et al. (1979)	X	
Caviahue	Tree rings	ARAR	1444	1974	530	37	71	LaMarche et al. (1979)	X	
Nalcas	Tree rings	ARAR	1386	1975	589	38	71	LaMarche et al. (1979)	X	
Tiuchue, Isla De Chiloe	Tree rings	FICU	1386	1987	601	42	73	LaMarche et al. (1979)	X	
Rio Cisne, Chubut	Tree rings	FICU	1338	1974	636	42	71	Lara et al. (2000)	X	
Lonco Luan	Tree rings	ARAR	1306	1974	668	38	65	LaMarche et al. (1979)	X	
Chenque Pehuen	Tree rings	ARAR	1246	1974	728	38	70	LaMarche et al. (1979)	X	
Piedra Del Aguila	Tree rings	ARAR	1200	1975	775	37	73	LaMarche et al. (1979)	X	
Primeros Pinos De Alumine	Tree rings	ARAR	1140	1974	834	38	70	LaMarche et al. (1979)	X	
San Gabriel	Tree rings	AUCH	1131	1975	844	33	70	LaMarche et al. (1979)	X	
El Asiento, Aconcagua	Tree rings	AUCH	1010	1976	966	37	71	LaMarche et al. (1979)	X	
Puerto Cafè	Tree rings	FICU	311	1992	1681	42	71	Lara et al. (2000)	X	
La Esperanza	Tree rings	FICU	–342	1995	2337	41	71	Lara et al. (2000)	X	
Cariaco Basin	Marine sediments		1222	1990	768	11	65	Black et al. (2007)	X	X
East Antarctica isotopic index	Ice cores		1200	1993	793	73	159	Goosse et al. (2004) and reference therein		X
Andean Glaciers – Huascaran dO18	Ice cores		1000	1984	984	9	77	Vimeux et al. (2009)		X
Andean Glaciers – Sajama dO18	Ice cores		1000	1984	984	18	68	Vimeux et al. (2009)		X
Andean Glaciers – Quelcaya dO18	Ice cores		1000	1984	984	14	71	Vimeux et al. (2009)		X
laguna Aculeo	Lake sediments		857	1997	1140	34	71	von Gunten et al. (2009)	X	X
Lago Frias	Lake sediments		1649	2006	357	42	72	Chapron (unpublished)		X
Potrok lake	Lake sediments		414	2000	1586	52	70	Haberzettl et al. (2005)		X

CPD
7, 153–198, 2011

Table 2. Calibration and validation statistics for the SAM. Median values are given with their 95% confidence intervals.

Region	R	R^2	RE
PG	0.68 (0.56, 0.83)	0.42 (0.22, 0.65)	0.35 (0.14, 0.57)
PM	0.62 (0.49, 0.81)	0.39 (0.21, 0.63)	0.3 (0.12, 0.52)
ST	0.65 (0.49, 0.76)	0.40 (0.22, 0.56)	0.33 (0.14, 0.50)
ANDES	0.65 (0.57, 0.76)	0.34 (0.15, 0.52)	0.20 (−0.13, 0.44)
SSA	0.65 (0.49, 0.80)	0.39 (0.21, 0.61)	0.31 (0.18, 0.51)

CPD
7, 153–198, 2011

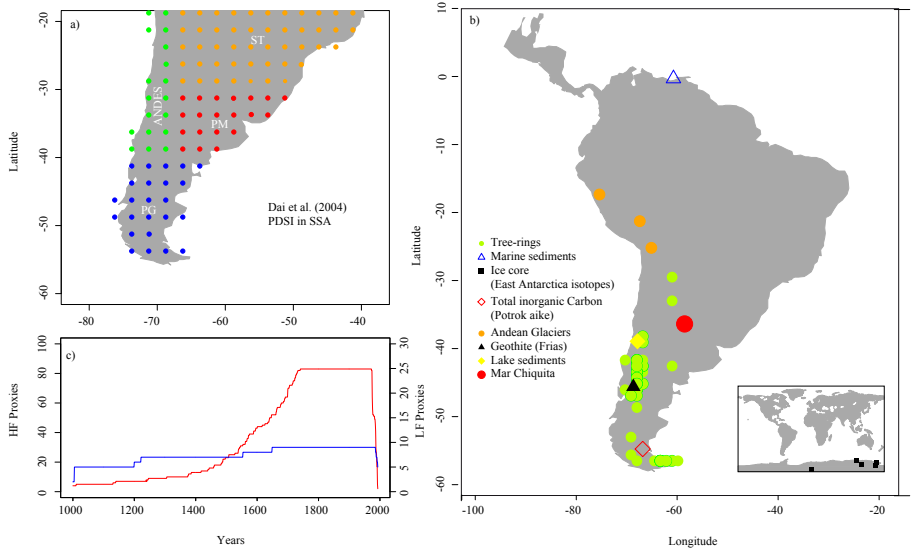

Fig. 1. Proxy and PDSI data used in this analysis. Position of Dai et al. (2004)'s 2.5×2.5 degrees PDSI in SSA **(a)**. Location and type of proxys used in this reconstruction **(b)**. Evolution of the number of LF ($0<f<0.08$) and HF ($0.08<f<0.5$) series used for the reconstruction **(c)**.

CPD
7, 153–198, 2011

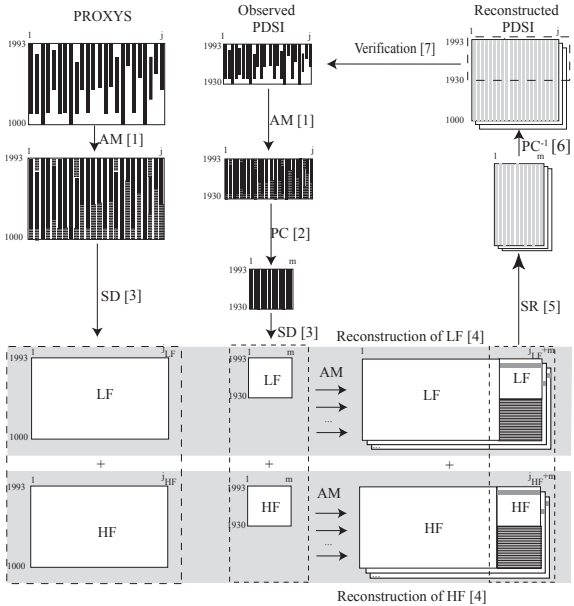

Fig. 2. Summary of the spectral analogue method. Missing values in the proxy and summer PDSI matrix are filled with the analogue method (AM [1]). The PDSI are reduced to m principal components. (PC [2]). Proxy and PDSI (PC) series are decomposed into their LF ($0<f<0.08$) and HF ($0.08<f<0.5$) components using a Fast Fourier Transform procedure (SD [3]). The reconstruction for each band is achieved using the AM [4]. This is done iteratively 100 times, and at each iteration, a random year t is removed for the calculation of validation statistics. Around year t, the ($t-4$, $t+4$) surrounding years are excluded as potential analogues. This h-block procedure is particularly useful in situations, like LF series, where there exists a large autocorrelation between years, causing the best analogues to be systematically located before of after year t. At each iteration, the reconstructed HF and LF bands are summed up to recompose (SR [5]) the full spectra of each PC. The PC are back-transformed into the original PDSI series using and inverse PC procedure (PC^{-1}, [6]). The reconstructed series are finally verified against observations (Verification [7]).

CPD
7, 153–198, 2011

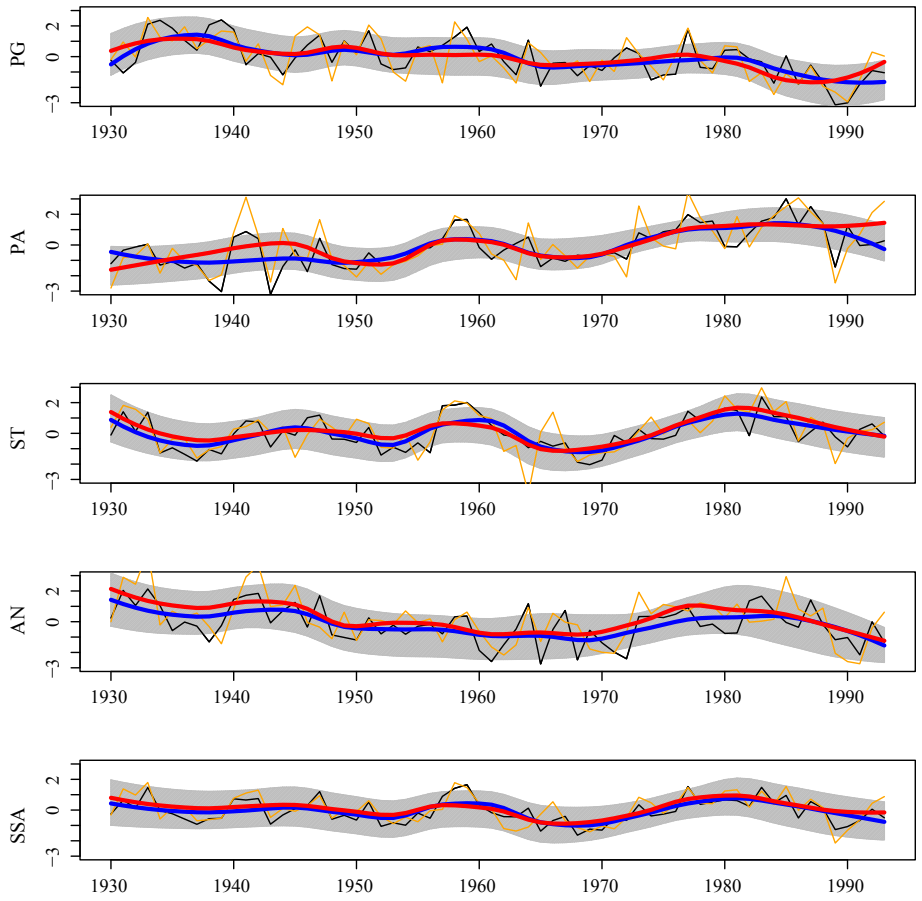

Fig. 3. Comparison between observed (red-orange) and reconstructed (blue-black) summer PDSI series for each region of SSA during the calibration period (1930–1993). Bold lines are loess smoothings. The 95% confidence intervals correspond to the gray zones.

CPD
7, 153–198, 2011

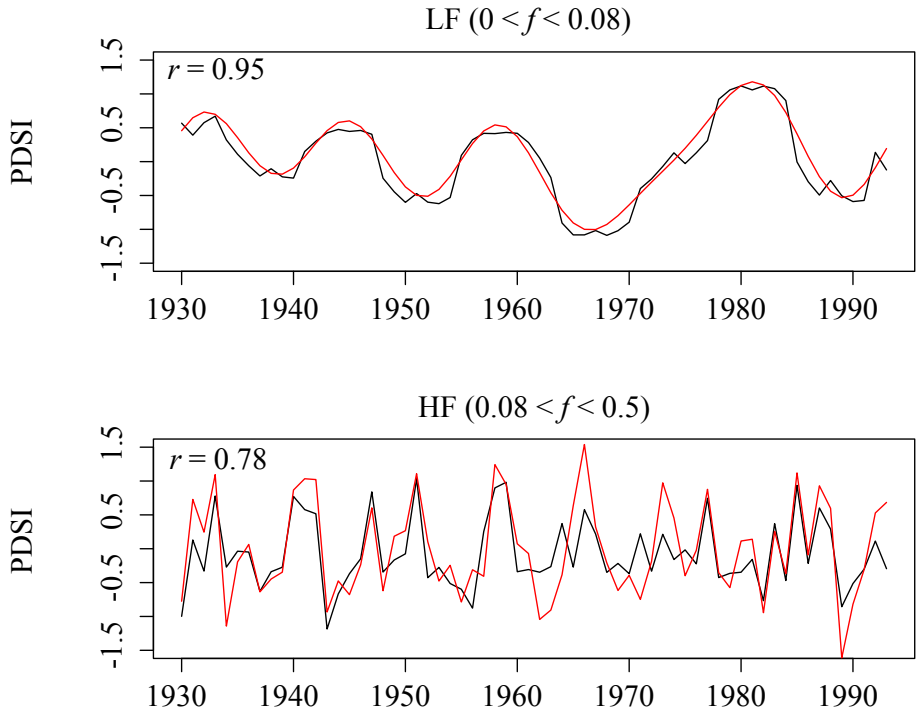

Fig. 4. The LF and HF components of the summer PDSI reconstruction for SSA. Observed and reconstructed values are in red and black, respectively.

CPD
7, 153–198, 2011

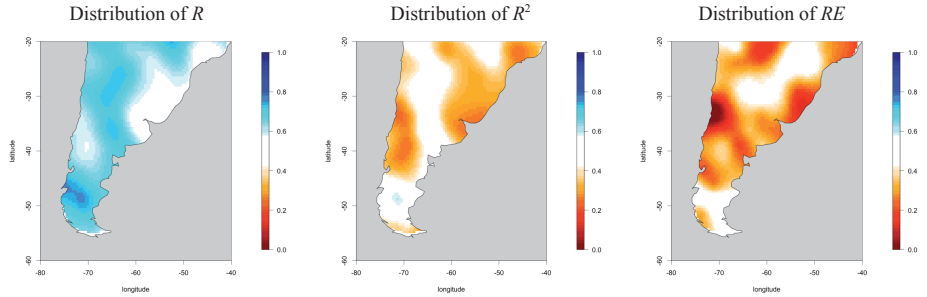

Fig. 5. Distribution of R, R^2 and RE statistics in SSA.

CPD
7, 153–198, 2011

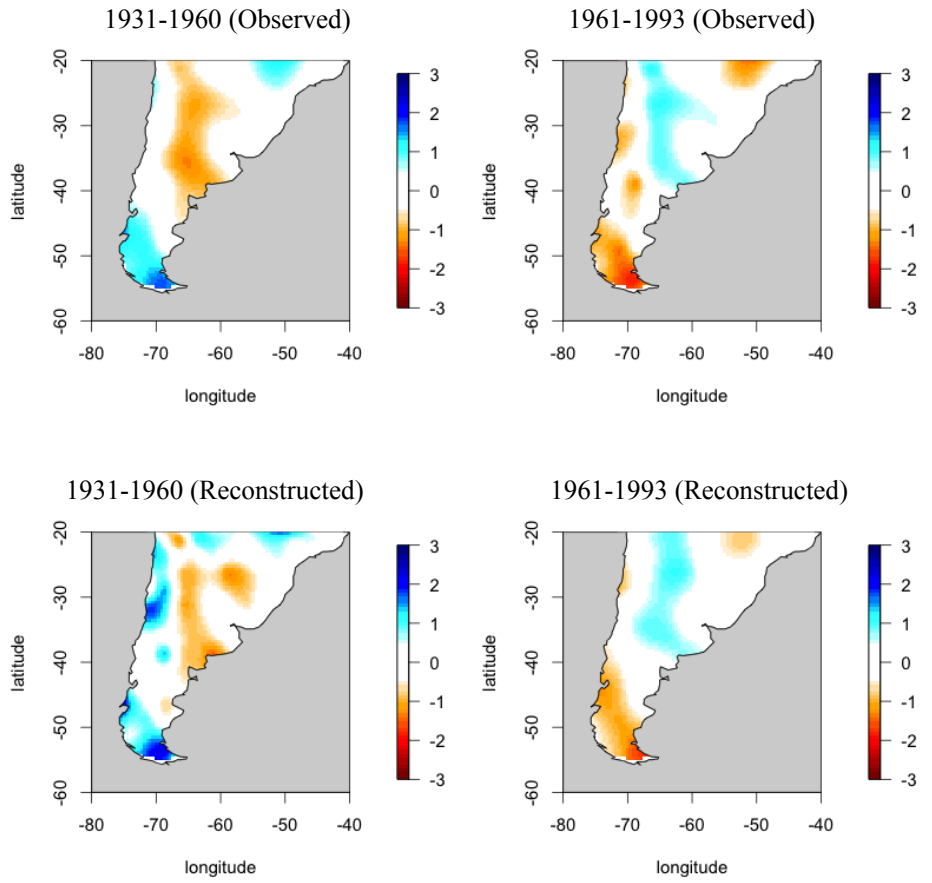

Fig. 6. Spatial comparison between observed (up) and reconstructed (down) summer PDSI values for two contrasted ~30 year periods: 1931–1960 (left) and 1961–1993 (right).

CPD
7, 153–198, 2011

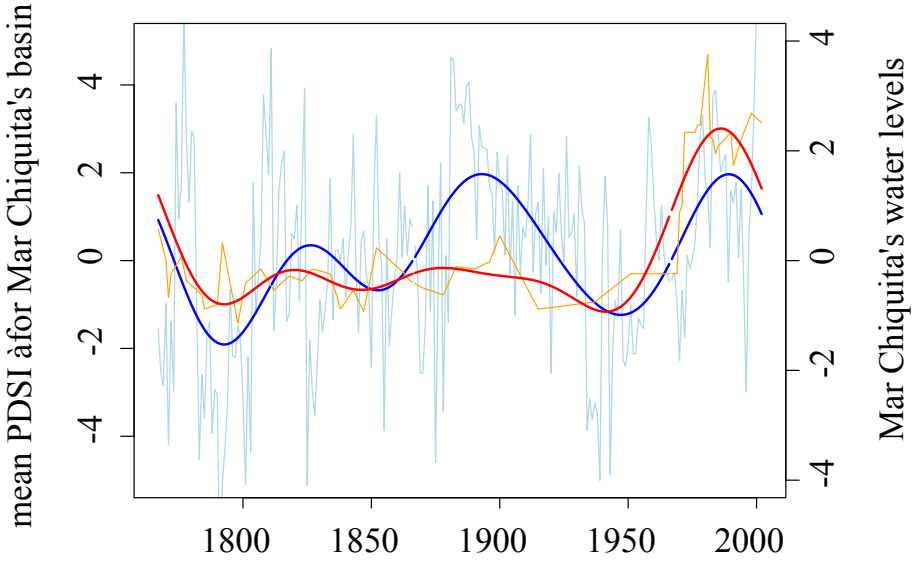

Fig. 7. Comparison of summer PDSI series (blue and light blue) with historical water levels (red and orange) of the laguna Mar Chiquita, Argentina (Piovano, 2002). Lake levels are shown wrt. to the level of the 1976–1977 shoreline. The smooth lines correspond to low pass ($f \leq 0.02$) filters. The summer PDSI series is an average covering the laguna's watershed.

CPD
7, 153–198, 2011

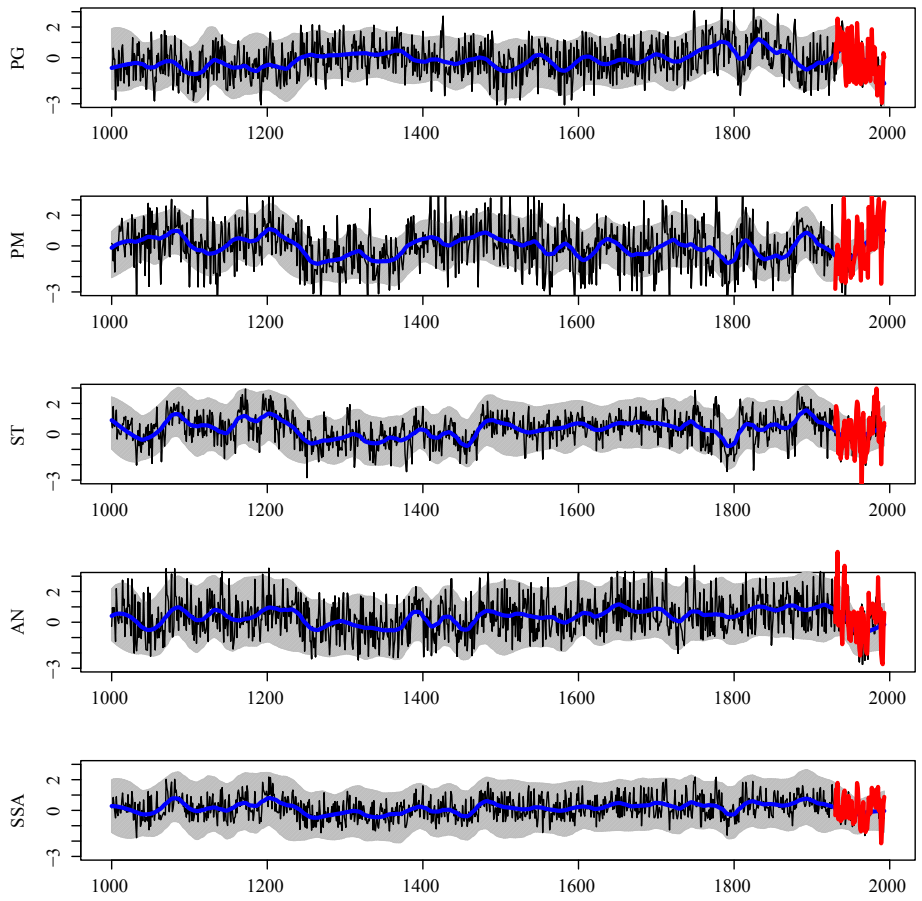

Fig. 8. Millennial summer PDSI reconstructions for each region of SSA. The observations are in red and reconstructions are in blue. Bold lines are loess smoothers and the gray shading correspond to the 95% confidence intervals.

CPD
7, 153–198, 2011

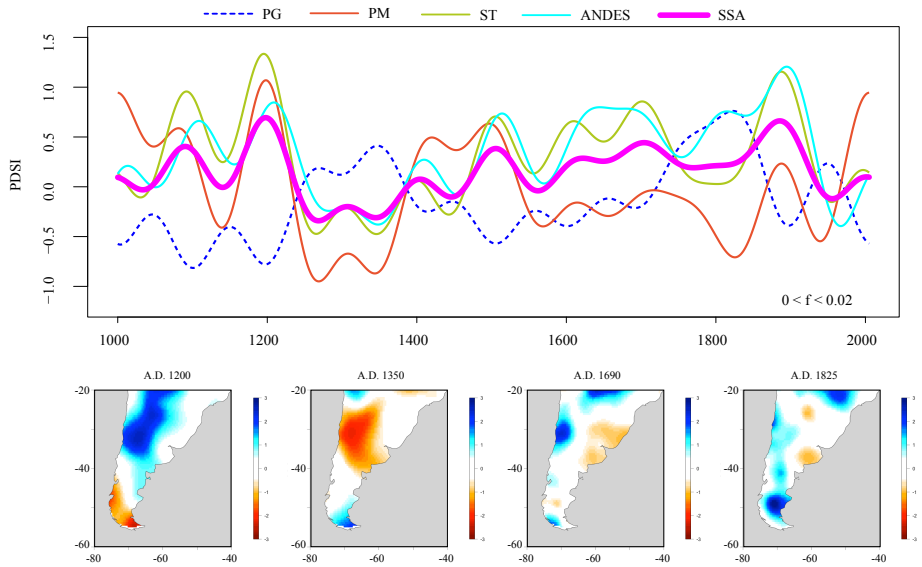

Fig. 9. Smoothed summer PDSI reconstruction for each region of SSA emphasizing the antiphase between PG and the rest of the continent. Smooth lines correspond to 50 years low pass filters ($f \leq 0.02$). Example maps of 30 year periods centered on A.D. 1200, 1350, 1690 and 1825 are shown.

CPD
7, 153–198, 2011

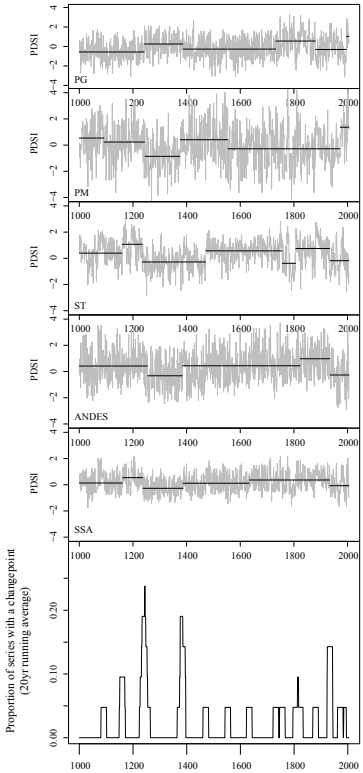

Fig. 10. Regime shift detection in summer PDSI series in SSA. The analysis was performed using the Rodionov (2004) method. To be detected, a regime needs to be at least 50 year long. If a regime has less than 50 years, the method can still allow for its detection, however, the significance required to determine that a date corresponds to a changepoint is adjusted to be inversely related to the length of the regime. The lower part of each graphs corresponds to the 20 year running average of the number of series recording a changepoint at year t. It gives a general idea of where these changepoints cluster in time.

CPD
7, 153–198, 2011

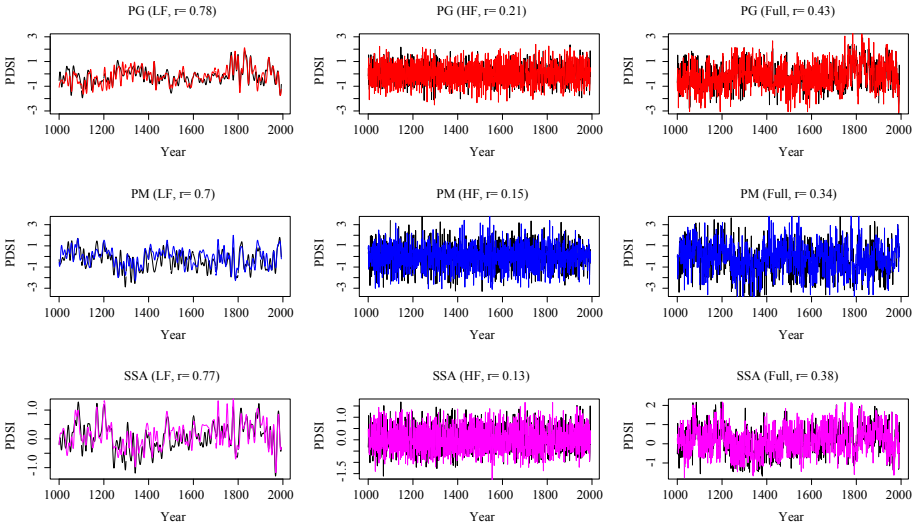

Fig. 11. Comparison between the reconstructions made from the full proxy dataset (colored lines, same colors as Fig. 8) and the reconstructions performed from only the proxies that go further than AD 1250 (in black). The left and center columns present the LF and HF components, respectively, while the right column depicts the comparison over the full spectra. Correlation coefficients (r, N=994) are shown in the title, for each frequency band and for each region. Not shown here: ANDES (r=0.28, for the full spectra) and ST (r=0.57, for the full spectra).

CPD
7, 153–198, 2011

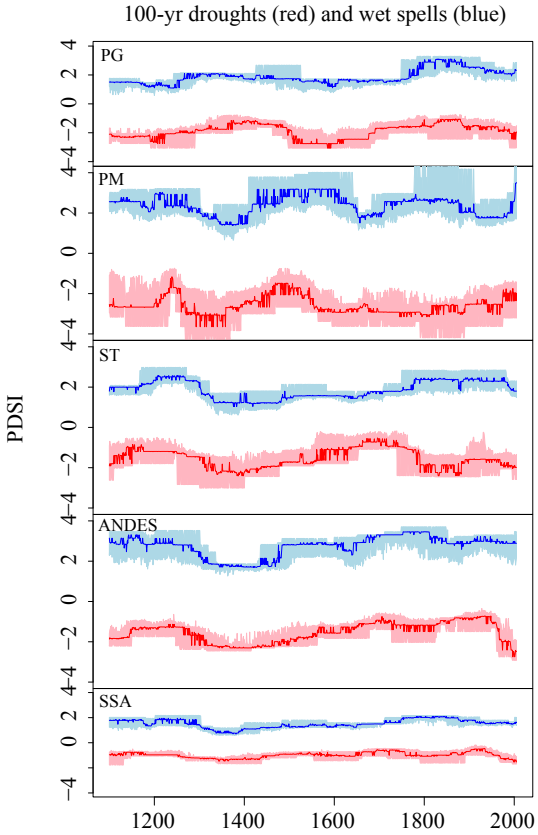

Fig. 12. Evolution of the summer PDSI values of the 100-year droughts (red) and wet spells (blue). For each year t, the analysis was conducted by considering the last 100 years. Fifty years were randomly chosen from the previous 100 years and the percentiles 0.01 (for the 100 year droughts) and 0.99 (for the 100 year wet spells) were chosen, considering that the probability of exceedance of a drought event=1/return period and a wet spell=1−(1/return period).

CPD
7, 153–198, 2011

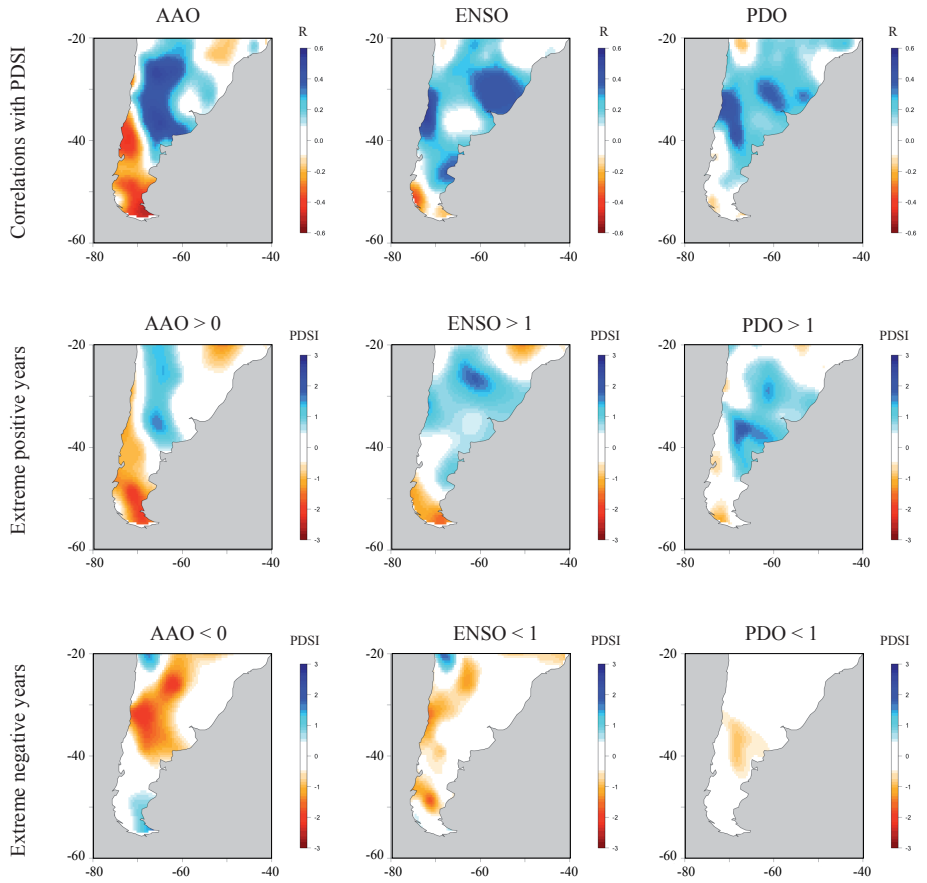

Fig. 13. Correlations of reconstructed summer PDSI with the main ocean-atmosphere indices: AAO, ENSO, and PDO (upper panel). The summer PDSI patterns displayed during extreme positive (middle panel) and extreme negative (lower panel) AAO, ENSO and PDO years.

CPD
7, 153–198, 2011

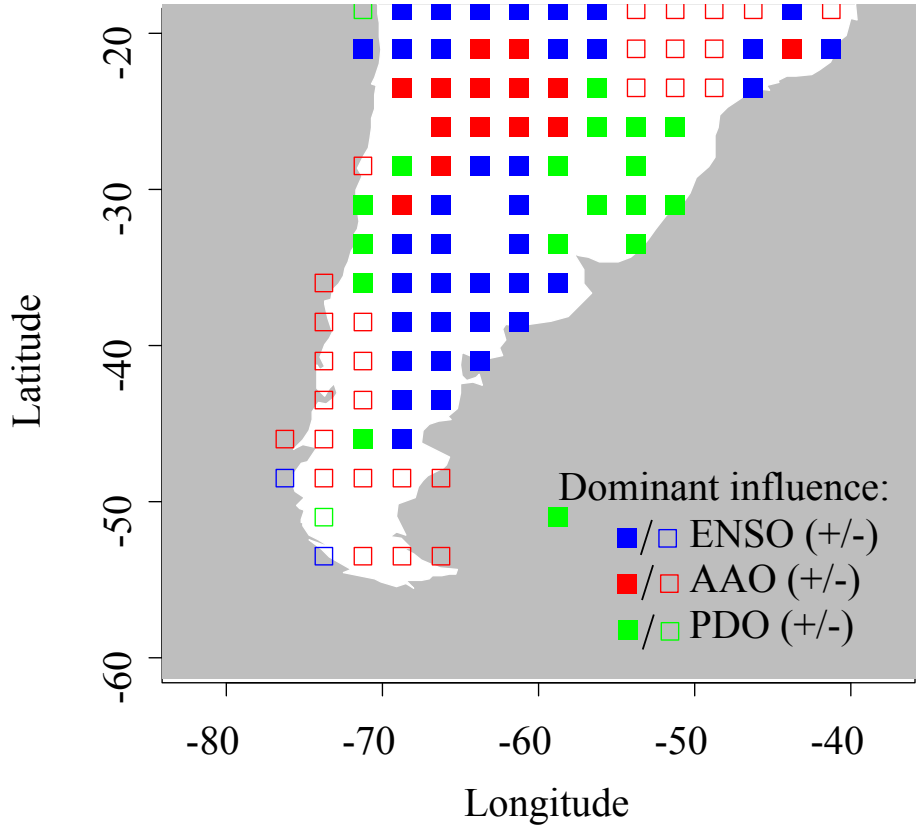

Fig. 14. Map of the magnitude and direction of the dominant influence, (measured as the magnitude and sign of the largest regression coefficient in the following equation: PDSI= a(AAO)+b(ENSO)+c(PDO)). Red symbols represent a dominant AAO influence while blue and green symbols indicate a dominant ENSO or PDO influence, respectively. Bold (empty) squares denote a positive (negative) influence on summer PDSI. The regression was performed for the longest common period (1950–2005).

CPD
7, 153–198, 2011

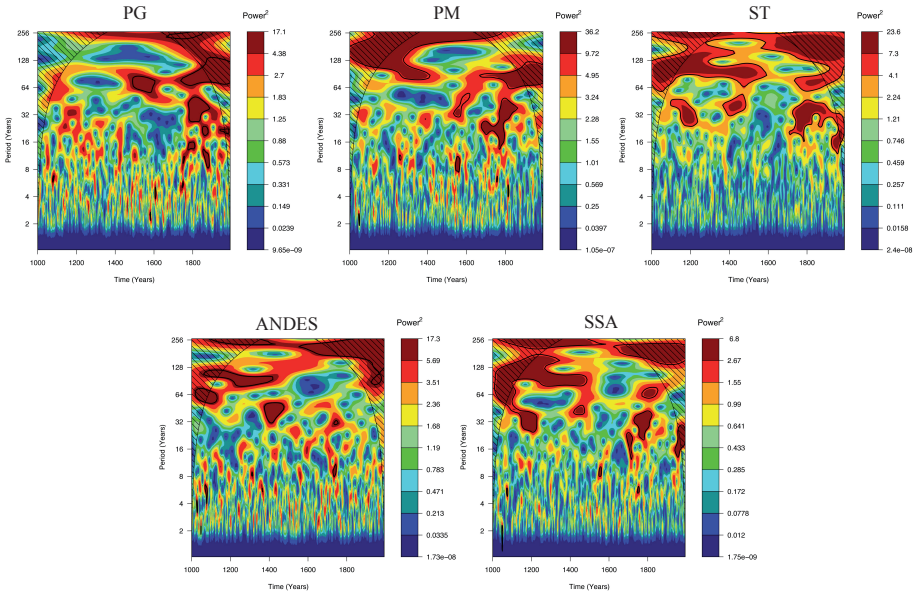

Fig. 15. Spectrograms depicting the relative importance (Power^2) of each periodicity (here, from 1 year to 256 years) in each region of SSA. The spectrograms were constructed using a continuous (Morlet) wavelet transform.

CPD
7, 153–198, 2011

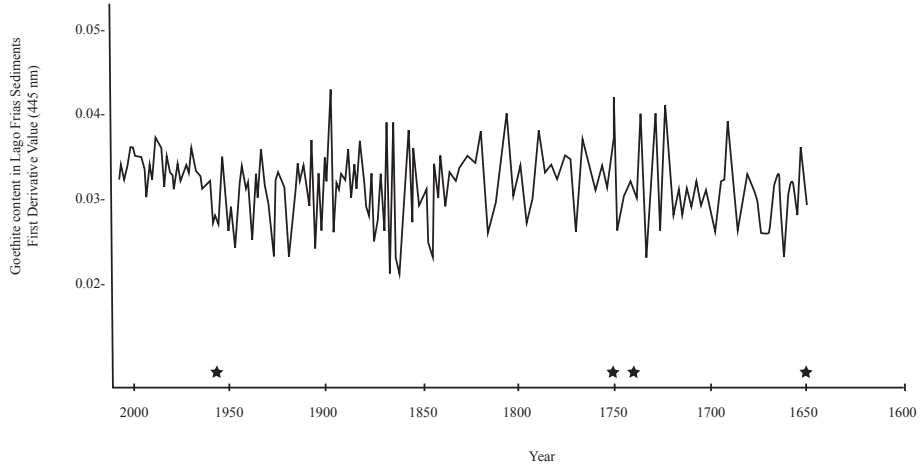

Fig. A1. Goethite (derivative 445 nm) chronology of Lago Frias varved lake sediments. Stars represent some well-known earthquakes in the area (AD 1960; AD 1751 and AD 1737).

CPD
7, 153–198, 2011

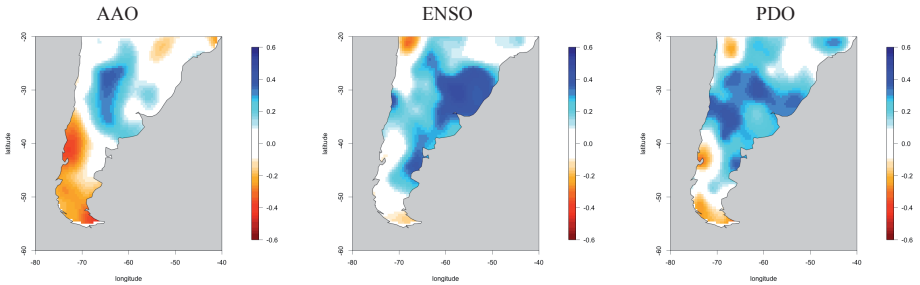

Fig. A2. Correlations of observed summer PDSI with the main ocean-atmosphere indices: AAO, ENSO, and PDO.

CPD
7, 153–198, 2011